



# Semi-convection in the ocean and in stars: A multi-scale analysis

FRIEDRICH KUPKA<sup>1\*</sup>, MARTIN LOSCH<sup>2</sup>, FLORIAN ZAUSSINGER<sup>3</sup> and THOMAS ZWEIGLE<sup>2,4</sup>

<sup>1</sup>Fakultät für Mathematik, Universität Wien, Austria

<sup>2</sup>Alfred-Wegener-Institut, Helmholtz Zentrum für Polar- und Meeresforschung, Bremerhaven, Germany

<sup>3</sup>Dept. Aerodynamics and Fluid Mechanics, BTU Cottbus-Senftenberg, Germany

<sup>4</sup>Fraunhofer-Institut für Kurzzeitdynamik, Ernst-Mach-Institut, Freiburg, Germany

(Manuscript received August 5, 2014; in revised form January 20, 2014; accepted February 2, 2015)

## Abstract

Fluid stratified by gravitation can be subject to a number of instabilities which eventually lead to a flow that causes enhanced mixing and transport of heat. The special case where a destabilizing temperature gradient counteracts the action of a stabilizing gradient in molecular weight is of interest to astrophysics (inside stars and giant planets) and geophysics (lakes, oceans) as well as to some engineering applications. The detailed dynamics of such a system depend on the molecular diffusivities of heat, momentum, and solute as well as system parameters including the ratio of the two gradients to each other. Further important properties are the formation and merging of well-defined layers in the fluid which cannot be derived from linear stability analysis. Moreover, the physical processes operate on a vast range of length and time scales. This has made the case of semi-convection, where a mean temperature gradient destabilizes the stratification while at the same time the mean molecular gradient tends to stabilize it, a challenge to physical modelling and to numerical hydrodynamical simulation. During the MetStröm project the simulation codes ANTARES and MITgcm have been extended such that they can be used for the simulations of such flows. We present a comparison of effective diffusivities derived from direct numerical simulations. For both stars and the oceanic regimes, the Nusselt numbers (scaled diffusivities) follow similar relationships. Semi-convection quickly becomes inefficient, because the formation of layers limits vertical mixing. In contrast to the complementary saltfingering, these layers tend to damp instabilities so that effective diffusivities of salinity (concentration) are up to two orders of magnitudes smaller than in the former case.

**Keywords:** hydrodynamics, numerical simulation, turbulence

## 1 Introduction

The purpose of this work was to calculate the semi-convection – and saltfinger – driven turbulent fluxes of temperature and salinity following previous saltfinger studies by FLEURY and LUECK (1991); RADKO (2003) and SCHMITT (1988, 2005). Then, these fluxes were used to determine the parametrization for the effective diffusivities of temperature  $K_T$  and salinity  $K_S$ . These parameters are frequently used in estimations of the vertical transport of temperature (or, actually, heat) and salinity in large scale models. Such an approach is mainly taken because of its convenience, since extra diffusion is simple to implement and stabilizes hydrodynamical models. From a physical point of view, the assumption may not hold that the thermodynamical state of the background stratification, which is driving vertical transport through a mean gradient, is changing only by a small amount along the typical mean free path in the flow. A fluid parcel advected through a convection zone may be subject to quite different conditions at the bottom of a zone in

comparison with its top which can limit the applicability of such parametrizations.

Hence, parametrizations in terms of diffusivities require thorough studies and awareness about their possible limitations. Direct Numerical Simulations (DNS) are necessary to achieve that goal. Before we sketch the layout of this paper, we first discuss the basic physics, previous research, and the motivation for studies on double diffusive convection.

Double diffusion in two-component fluids is a process where the differential molecular diffusion of the fluid components acts on different time scales. The thermal diffusion is generally faster than the diffusion of concentration, because the latter involves material concentration transport by random Brownian motion while the former is the transport of kinetic energy through molecular collisions. In a statically stable stratification (density increases with depth of the fluid), there are two situations in which double diffusion processes can destabilize the fluid and lead to mixing beyond the molecular scales: salt fingering and semi-convection or diffusive convection.

For oceanographic salt fingering (STERN, 1960), warm and saline (high concentration) water needs to be

\*Corresponding author: Friedrich Kupka, Fakultät für Mathematik, Universität Wien, Oskar-Morgenstern-Platz 1, 1090 Wien, Austria, e-mail: Friedrich.Kupka@univie.ac.at

stacked over cold and fresh (low concentration) water. This situation, where the salinity gradient destabilizes the water column, but is balanced by the temperature gradient, is observed in the Caribbean (SCHMITT, 2005) or the Gulf of Lyon in the Mediterranean Sea (ONKEN and BRAMBILLA, 2003; ZODIATIS and GASPARINI, 1996). When small perturbations at the layer interface move a warm, saline water parcel into the cold and fresh environment below, it quickly loses heat by fast thermal diffusion. The salt diffusion is 100 times slower so that the salinity in the water parcels remains unchanged. The now cold and saline water parcel has lost its buoyancy and is accelerated further downward feeding the instability. In the same way, a cold and fresh water parcel from the lower layer gains buoyancy when it is moved upwards and warms through diffusion.

The astrophysical equivalent of salt fingering convection is often also discussed under the more general name of *thermohaline convection*. Both terms refer to the scenario of a stable temperature gradient counteracted by a destabilizing gradient in mean molecular weight. In astrophysics, this can occur in late stages of stellar evolution (off-centre shell burning, a case first described in THOMAS, 1967) or due to accretion of heavy material near the stellar surface (STOTHERS and SIMON, 1969).

The semi-convection case in stars and in oceans requires the opposite stratification. The concentration gradient with high concentration below low concentrations stabilizes the temperature gradient when fluid with lower temperatures is stacked above fluid with higher temperatures. In stars (e.g. ZAUSSINGER et al., 2013, for a review), such a stratification appears frequently within regions of nuclear burning (nuclear fusion), for instance, in the core of massive stars where hydrogen gets converted into helium at a high rate through the so-called CNO cycle. The increase of the amount of helium, which has a higher mean molecular weight than hydrogen, in the centre can lead to a gradient stabilizing the fluid against the destabilizing temperature gradient. By triggering convective mixing the latter usually leads to a core region with homogeneous composition. But near the upper boundary of that region a stabilizing (helium) concentration gradient will form and it is the structure and time evolution of this transition region, characterized by “inefficient” or “semi-” convection that has been debated since the early work of SCHWARZSCHILD and HÄRM (1958). In the interior of (gaseous) giant planets such as Jupiter or Saturn a similar stratification favoring semi-convection is expected to occur (STEVENSON, 1985; LECONTE and CHABRIER, 2012; LECONTE and CHABRIER, 2013). In this case, heavy elements contribute a much larger fraction of mass to the fluid in the deep interior of the planet than found for its atmosphere layers. There, semi-convection is rather caused by the initial formation process of the object and alters its evolution over very long timescales (LECONTE and CHABRIER, 2012; LECONTE and CHABRIER, 2013).

The expression semi-convection has thus far been used only in astrophysics. Oceanographers describe the

same scenario as *diffusive convection*. Since this expression can more easily be confused and wrongly applied to other scenarios (such as the case where both temperature and concentration gradient are stable, but the fluid may nevertheless be mixed by non-local entrainment of fluid from a convectively unstable zone nearby), we use its astrophysical equivalent here and in the following.

In the Arctic ocean, the so-called cold halocline represents a condition for semi-convection. On smaller scales, melting sea-ice also generates fresh and cold water over warmer and more saline water. Given such stratification, fast thermal diffusion erodes the temperature gradient at the interface of the layers. Once the interface is destabilized warm and saline fluid parcels move up into a cold environment where they quickly lose heat and thus buoyancy again through fast thermal diffusion and are accelerated downwards. By the same token, cold and fresh fluid parcels can move down where they gain buoyancy again and return upwards. Obviously, the sources of instability are much smaller in semi-convection than in salt fingering and mostly confined to boundary layers between regions with different chemical composition. As a consequence, vigorous semi-convection requires a background stratification that is only marginally stable.

Oceanic semi-convection has received very little attention in the past (VERONIS, 1965). For example, LINDEN (1974) calculated flux ratios of salinity and temperature for semi-convection analytically and compared the results to experimental data (TURNER, 1965). A few oceanic measurements in the Adriatic Sea (CARNIEL et al., 2008) and near melting icebergs (TURNER, 2010) demonstrated the relevance of semi-convection to vertical mixing and stability. Until recently, there have virtually been no numerical simulation studies that address semi-convection in the ocean. Saltfingers in lab experiments, field observations, and numerical simulations have been described in numerous contexts (e.g. HUPPERT and MOORE, 1976; SCHMID et al., 2010; FLEURY and LUECK, 1991; RADKO, 2003; SCHMITT, 1988, 2005). In a recent study, TRAXLER et al. (2011) and MIROUH et al. (2012) compare oceanic and astrophysical salt fingering and semi-convection. FLANAGAN et al. (2013) have studied the formation of layers in the Arctic Sea caused by semi-convection.

In the following Section 2 we first introduce the basic equations describing the dynamics of physical systems with double diffusive convection: the Navier–Stokes equations for a compressible fluid coupled to a concentration equation and several variants of the Boussinesq approximation to them which are suitable either for a perfect gas or for liquids. In addition, we introduce physical quantities of interest used in studying the fluxes of heat and concentration and hence mixing in such systems. We also give further definitions. In Section 3 we describe the simulation codes used in our work and provide a brief overview on their underlying mathematical and physical concepts. Our key results are collected in Section 4, that is, the computation and parametrization

of effective diffusivities for the cases we have studied. Section 5 presents our conclusions.

## 2 Semi-convection and salt-fingering

We first recall the dynamical equations describing the time evolution of a two-species fluid and several variants of the Boussinesq approximation to them which we have used in practice. The equivalence of these variants, as used in both ANTARES and MITgcm, is discussed. We then define physical quantities and the main parameters as well as related notation used to describe physical systems for which double-diffusive convection occurs and briefly discuss some basic physics of semi-convection and salt-fingering.

### 2.1 The basic equations

A two-species flow for which double-diffusive convection occurs is modelled by the Navier–Stokes equations and related conservation laws. They can be recast as

$$\frac{\partial}{\partial t} \begin{pmatrix} \rho \\ \rho c \\ \rho \mathbf{u} \\ e \end{pmatrix} = -\nabla \cdot \begin{pmatrix} \rho \mathbf{u} \\ \rho c \mathbf{u} \\ \rho \mathbf{u} \otimes \mathbf{u} + P - \sigma \\ e \mathbf{u} + P \mathbf{u} - \mathbf{u} \cdot \sigma \end{pmatrix} + \begin{pmatrix} 0 \\ 0 \\ \rho \mathbf{g} \\ \rho \mathbf{g} \cdot \mathbf{u} \end{pmatrix} + \nabla \cdot \begin{pmatrix} 0 \\ 0 \\ \rho \kappa_c \nabla c \\ 0 \\ K \nabla T \end{pmatrix}. \quad (2.1)$$

Here,  $P$  is the product of the scalar pressure  $p$  with the unit tensor  $\mathbf{I}$  (which in index notation for a tensor of rank two is represented by Kronecker’s delta and hence  $\nabla \cdot P = \nabla \cdot p \mathbf{I} = \nabla p$ , the gradient of  $p$ ). The meaning of the other symbols is standard:  $\rho$  and  $c$  denote mass density and concentration,  $\mathbf{u}$  is the velocity and  $e$  the density of internal energy,  $\mathbf{g} = (0, 0, -g)^\top$  is the gravitational acceleration (which here only has a vertical component of magnitude  $g$  and  $^\top$  indicates the transposition of the vector), while  $t$  denotes time. Furthermore,  $\sigma$  is the viscous stress tensor,  $\kappa_c$  is the kinematic diffusivity of concentration while  $K$  is the heat (or radiative) conductivity which both depend on temperature  $T$  as well as on concentration and density. Here and in the following,  $0$  is used to represent zero without specifically mentioning whether it has the rank of a scalar, a vector, or tensor of rank two, as this follows from the specific context.

Since the velocities in flows of double-diffusive convection are often small compared to the speed of sound while the fluctuations of the dynamical variables are small compared to their mean value, the Boussinesq approximation to (2.1) can be used. This requires that the mean thermodynamical variables, in particular the pressure  $p$ , change only little along the vertical extent of the simulation domain (i.e. the domain height

is small in terms of the local pressure scale height<sup>1</sup>  $H_p = (-\partial \ln p / \partial z) \approx P / (\rho g)$ , where the latter holds for hydrostatic equilibrium).

In that case we may instead only consider the fluctuations of the thermodynamical variables ( $T$ ,  $p$ ,  $\rho$ ,  $c$  or, alternatively, salinity  $S$ ) and derive dynamical equations for the time evolution from the general fluid dynamical conservation laws for a fully compressible flow (2.1). To this end the potential temperature is introduced as an adiabatically filtered temperature,  $\Theta = T(p_0/p)^{(\gamma-1)/\gamma}$ , where  $p_0$  is a constant reference pressure and  $\gamma$  is the ratio of specific heats at constant pressure and volume. Thermodynamical variables  $f(t, \mathbf{x})$  such as  $\Theta(t, \mathbf{x})$  are split into a mean background state  $\bar{f}$  (an average over space and time) and its fluctuation  $f'$  around that value,  $f = \bar{f} + f'$ . Pressure fluctuations are expressed by considering hydrostatic equilibrium for the mean (background) variables. Taking the small thickness of the domain in terms of  $H_p$  into account and that the diffusivities vary but little in such a flow and finally that the flow velocities are small compared to local sound speed one eventually arrives (see SPIEGEL and VERONIS, 1960 or also, e.g., ZAUSSINGER, 2010 for a detailed discussion) at the Boussinesq approximation of (2.1):

$$\frac{\partial}{\partial t} \begin{pmatrix} S' \\ \mathbf{u} \\ \Theta' \end{pmatrix} = -\nabla \cdot \begin{pmatrix} \mathbf{u}(\bar{S} + S') \\ \mathbf{u} \otimes \mathbf{u} + \frac{p'}{\rho_0} - \nu \nabla \mathbf{u} \\ \mathbf{u}(\bar{\Theta} + \Theta') \end{pmatrix} - \begin{pmatrix} 0 \\ (\frac{\Theta'}{\Theta_0} - \frac{S'}{S_0}) \mathbf{g} \\ 0 \end{pmatrix} + \nabla \cdot \begin{pmatrix} \kappa_S \nabla S' \\ 0 \\ \kappa_T \nabla \Theta' \end{pmatrix}. \quad (2.2)$$

which is completed by the incompressibility constraint

$$\nabla \cdot \mathbf{u} = 0. \quad (2.3)$$

Here, we have replaced the concentration  $c$  with salinity  $S$  and the same holds for their fluctuating variables  $c'$  and  $S'$  as well as their diffusivities:  $\kappa_S = \kappa_c$ , while  $\kappa_T = K / (c_p \rho)$  and  $c_p$  is the specific heat at constant pressure. The diffusivities  $\kappa_S$  and  $\kappa_T$  are assumed to be constant as is the kinematic viscosity  $\nu$ . Similar to (2.1)  $P'$  is the product of the scalar pressure fluctuation  $p'$  and the unit tensor  $\mathbf{I}$ . It is a tensor as is  $\nabla \mathbf{u}$ . The quantities  $\rho_0$ ,  $\Theta_0$  and  $S_0$  describe the constant background state. The contributions of kinematic viscosity to the equation of (potential) temperature can be neglected, since they are small for low Mach number flows including those cases for which the Boussinesq approximation applies (cf. also equations II–4–13 to II–4–25 in LESIEUR (1997)).

We would like to emphasize here that the fluctuations  $f'$  refer to a mean background state which is constant

<sup>1</sup>We note that typical values for this quantity range from 100 km near the surface of the solar convection zone to about 50000 km near its bottom, while it is found to be about 8 km in the lower part of the atmosphere of the Earth and increases from 10 m near the surface to several km near the bottom of an ocean.

with respect to horizontal spatial coordinates and for the cases considered here also constant as a function of time. No separate notation is used here to distinguish these quantities from turbulent fluctuations around some (possibly differently specified) mean. Rather, we consider the fluctuations  $f'$  synonymous with turbulent fluctuations for which the mean state is given by the Boussinesq reference state.

For constant temporal and spatial averages of the potential temperature and salinity, we have  $\partial\bar{S}/\partial t = 0$ ,  $\partial\bar{\Theta}/\partial t = 0$ ,  $\nabla\bar{S} = 0$ , and  $\nabla\bar{\Theta} = 0$ , whence we can rewrite (2.2) into the form used in ANTARES,

$$\frac{\partial}{\partial t} \begin{pmatrix} S \\ \mathbf{u} \\ \Theta \end{pmatrix} = -\nabla \cdot \begin{pmatrix} \mathbf{u} \otimes \mathbf{u} + \frac{\rho'}{\rho_0} \mathbf{u} S \\ \mathbf{u} \Theta \end{pmatrix} - \begin{pmatrix} 0 \\ (\frac{\rho'}{\Theta_0} - \frac{S'}{S_0}) \mathbf{g} \\ 0 \end{pmatrix} + \nabla \cdot \begin{pmatrix} \kappa_S \nabla S \\ 0 \\ \kappa_T \nabla \Theta \end{pmatrix} \quad (2.4)$$

which is to be solved together with the incompressibility constraint (2.3). We refer to this set of equations for the case of the Boussinesq approximation if a perfect gas equation of state actually holds for the fluid.

The case of water is more easily dealt with using a slightly different form of these equations. It can also be directly derived from (2.1) without assuming a hydrostatic background state and for the case of a realistic equation of state, for instance, as in McDougall et al. (2003). This is the form of the Boussinesq approximation actually used in MITgcm for all the simulation runs discussed in this paper. It features an equation for  $T$  instead of  $\Theta$  and reads:

$$\frac{\partial}{\partial t} \begin{pmatrix} S \\ \mathbf{u} \\ T \end{pmatrix} = -\nabla \cdot \begin{pmatrix} \mathbf{u} \otimes \mathbf{u} + \frac{\rho'}{\rho_0} \mathbf{u} S \\ \mathbf{u} T \end{pmatrix} + \begin{pmatrix} 0 \\ (\frac{\rho'}{\rho_0}) \mathbf{g} \\ 0 \end{pmatrix} + \nabla \cdot \begin{pmatrix} \kappa_S \nabla S \\ 0 \\ \kappa_T \nabla T \end{pmatrix}. \quad (2.5)$$

We emphasize that both ANTARES and MITgcm consider a complete equation state (perfect gas or water) for either the mean background state when assuming (2.4) to hold or for the local thermodynamical state required to be known in (2.1) and in (2.5). Linear stability analyses, however, consider a linearized form of the equation of state, i.e.

$$\rho = \rho_0(1 - \alpha(T - T_0) + \beta(S - S_0)). \quad (2.6)$$

The thermal expansion coefficient  $\alpha = (-1/\rho)(\partial\rho/\partial T)$  and the solutal contraction coefficient  $\beta = (1/\rho)(\partial\rho/\partial S)$  are evaluated in (2.6) for a thermodynamical reference state  $(T_0, S_0, p_0)$ . Since we consider low Mach number flows with small fluctuations of the dynamical variables relative to either mean reference states or horizontal averages, the differences between the complete equation of states and their linearized form should be small, a prerequisite for applicability of the stability analyses.

## 2.2 Double-diffusive convection

### 2.2.1 General remarks

The magnitude of the turbulent fluxes for semi-convective and salt-fingering systems depends on the Lewis number ( $Le = \kappa_S/\kappa_T$ , the ratio of the molecular diffusivities of concentration and heat), the Prandtl number ( $Pr = \nu/\kappa_T$ , the ratio of kinematic viscosity and heat diffusivity), and the stratification, characterized by a stability parameter: the ratio  $R_\rho^{sc}$  of concentration and temperature gradients.

We recall that within the Boussinesq approximation the thermal Rayleigh number  $Ra_T$ , a corresponding solute Rayleigh number  $Ra_S$  and the stability parameter  $R_\rho^{sc}$  are defined as  $Ra_T = g\alpha(T_{\text{bottom}} - T_{\text{top}})D^3/(\kappa_T\nu)$ ,  $Ra_S = g\beta(S_{\text{bottom}} - S_{\text{top}})D^3/(\kappa_T\nu)$  and  $R_\rho^{sc} = Ra_S/Ra_T$ .  $D$  is the length scale to which the Rayleigh numbers refer to (the size of the simulation domain, the thickness of a layer, etc.) whereas temperatures  $T$  and salinities  $S$  are taken at the bottom and top of the domain which in turn are just a distance  $D$  separated from each other. The ratio  $R_\rho^{sc}$  is particularly convenient for studying double-diffusive processes and is more frequently used than  $Ra_S$ . The superscript “sc” is used here to distinguish it from similar parameters and to stress its usefulness in discussing the stability properties of semi-convection.

Linear theory predicts semi-convection for the stability range  $1 \leq R_\rho^{sc} \leq \frac{1+Pr}{Le+Pr}$  (Baines and Gill, 1969; Stevenson, 1979; Zaussinger et al., 2013), but determining the actual magnitude of the turbulent fluxes as well as the effective diffusivities for semi-convective flows requires direct numerical simulations (DNS).

The conservation laws (2.1)–(2.5) are frequently transformed into a non-dimensional form for further analysis and also for their numerical solution. The Prandtl number  $Pr$ , the Lewis number  $Le$ , the thermal Rayleigh number  $Ra_T$ , the solute Rayleigh number  $Ra_S$ , and the stability parameter  $R_\rho^{sc}$  are common parameters used in such transformations and are also used in the following discussions. We note that for cases as in Section 2.1, where the diffusivities and viscosity are assumed to be constant,  $Pr$  and  $Le$  are constant as well.

We now discuss in more detail the two most interesting cases with the gradients of temperature and salinity counteracting instead of amplifying each other.

### 2.2.2 Semiconvection, stability and layering

Astrophysical systems such as stars or giant planets extend over many pressure scale heights  $H_p$ . It is hence common to express stability criteria by means of dimensionless, logarithmic gradients with respect to the (gas) pressure  $p$ . The standard notation for the gradients of temperature and mean molecular weight is  $\nabla := \partial \ln T / \partial \ln p$  and  $\nabla_\mu := \partial \ln \mu / \partial \ln p$  while the adiabatic temperature gradient is abbreviated as  $\nabla_{\text{ad}} := (\partial \ln T / \partial \ln p)_{\text{ad}}$ . In astrophysics the difference  $\nabla - \nabla_{\text{ad}}$ ,

known as the superadiabatic temperature gradient, is the usual quantity to determine whether a stratification is thermally stable. In geophysics the potential temperature  $\Theta$  is common for the same purpose. For the dimensionless gradient of potential temperature  $\nabla_{\Theta}$  and a perfect gas equation of state it is straightforward to show (for instance, ZAUSSINGER, 2010) that  $\nabla_{\Theta} = \nabla - \nabla_{\text{ad}}$ .

These quantities describe the dynamical stability of a system that is governed by the Brunt-Väisälä frequency (see, e.g., chapter 6 in KIPPENHAHN and WEIGERT (1991)). In general,  $N^2 := (g\delta/H_p)(\nabla_{\text{ad}} - \nabla + (\varphi/\delta)\nabla_{\mu})$ , where  $\delta = -(\partial \ln \rho / \partial \ln T)$  and  $\varphi = (\partial \ln \rho / \partial \ln \mu)$ . For a perfect gas this simplifies to  $N^2 = gH_p^{-1}(\nabla_{\mu} - (\nabla - \nabla_{\text{ad}}))$ . If  $N^2 > 0$ , a vertical displacement leads to a (usually damped) oscillation, while for  $N^2 < 0$  a vertical displacement leads to an exponentially growing instability and convection sets in. In a simplified form ( $\delta = \phi = 1$  for a perfect gas) this is known as the Ledoux criterion of convective stability (LEDoux, 1947):  $\nabla_{\mu} > \nabla - \nabla_{\text{ad}}$  implies stability while for  $\nabla - \nabla_{\text{ad}} > \nabla_{\mu}$  convection is predicted to set in. In the spirit of the Boussinesq approximation the same conditions can be written by comparing the solute and thermal Rayleigh numbers. With the above definitions of  $\text{Ra}_{\text{S}}$  and  $\text{Ra}_{\text{T}}$  (note that there are different conventions for choosing the sign),  $0 < \text{Ra}_{\text{S}} < \text{Ra}_{\text{T}}$  corresponds to the Ledoux unstable case and  $0 < \text{Ra}_{\text{T}} < \text{Ra}_{\text{S}}$  to the Ledoux stable case. These stability conditions are the result of a well established linear analysis (see Section 1). In their most simple form as is discussed here and sufficient for our work, it is assumed that both  $\text{Ra}_{\text{T}}$  and  $\text{Ra}_{\text{S}}$  are large and in this sense  $\nu$  is small. Otherwise, slightly more complex relations hold which feature additional explicit dependencies on  $\text{Pr}$  and  $\text{Le}$ . Evidently, for the Ledoux stable case,  $\text{R}_{\rho}^{\text{sc}} > 1$ , while for the unstable one,  $\text{R}_{\rho}^{\text{sc}} < 1$ . Staying within the framework of linear stability analysis, a layer where  $\text{R}_{\rho}^{\text{sc}} > 1$  is *dynamically stable*, but can be *vibrationally unstable* (KIPPENHAHN and WEIGERT, 1991): a (vertically) oscillating fluid element does not have the same temperature as its environment and exchanges heat with it, that is, it moves non-adiabatically. In a chemically homogeneous case ( $\nabla_{\mu} = 0$ ) this results in damped oscillations. In the non-homogeneous case ( $\nabla_{\mu} > 0$ ) the oscillations may either also be damped or they increase slowly (on the time scale of heat diffusion). The vibrationally unstable region is characterized by  $1 \leq \text{R}_{\rho}^{\text{sc}} \leq \frac{1+\text{Pr}}{\text{Le}+\text{Pr}}$  and it is this parameter regime the term *semiconvective* in astrophysics usually refers to (see, e.g., chapter 30.4.2 in KIPPENHAHN and WEIGERT (1991)).

Linear stability analysis, however, is a very limited tool for such conditions. CANUTO (1999), who gives a detailed discussion of the various stability criteria for semi-convection and salt-fingers, notes that the linear stability analysis does not account for turbulence and the consequences of transport of mass, heat, and concentration. A more complete analysis would actually introduce the *turbulent diffusivities*, or in our ter-

minology, *effective diffusivities*, into the stability criteria. The dynamically unstable case is characterized by  $\nabla - \nabla_{\text{ad}} > (K_{\text{S}}/K_{\text{T}})\nabla_{\mu}$  while the vibrationally unstable one requires  $(K_{\text{T}}/K_{\text{S}})(\nabla - \nabla_{\text{ad}}) > \nabla_{\mu} > (\nabla - \nabla_{\text{ad}})$ . Since the latter implies  $K_{\text{T}} > K_{\text{S}}$  for a consistent model, the unstable regime is expected to extend somewhat into the region where  $\text{R}_{\rho}^{\text{sc}} > 1$ . Applicability of the so-called Schwarzschild criterion of convective stability (SCHWARZSCHILD, 1906), where  $\nabla > \nabla_{\text{ad}}$  describes an unstable state and  $\nabla < \nabla_{\text{ad}}$  a stable one, is found to have to remain limited to where  $\nabla_{\mu} = 0$ , since only in this case once can expect  $K_{\text{S}} = 0$ . At the bottom line, the mixing efficiency is found to be overestimated when imposing only the Schwarzschild criterion  $\nabla > \nabla_{\text{ad}}$  in stellar evolution calculations while it is underestimated when requiring the Ledoux criterion  $\text{R}_{\rho}^{\text{sc}} < 1$  for convective mixing to occur. The complete model (CANUTO, 1999, 2011) predicts a mixing efficiency that is in-between the naive application of the two criteria and cannot be retrieved from linear stability analysis alone. We note that the discussion of CANUTO (1999, 2011) is made with a specific model approximation in mind, a Reynolds stress description of the entire fluid domain which would usually be applied in low resolution global models of oceans or stars which necessarily average over separate double-diffusive layers (when present). In limiting cases of the full model diffusivities and gradient expressions for the fluxes appear and provide the framework for his discussion. It is quite remarkable that other theoretical analyses which have quite different starting points such as the description of individual layers to which we turn in the following arrive at similar conclusions. Of course, since all these discussions are to some extent model dependent, they require confirmation by experiments or direct numerical simulation.

An important phenomenon that is not found from linear stability analysis either is the formation of layers in the Ledoux stable case. With a non-linear analysis PROCUTOR (1981) was able to show that in a region limited by

$$1 \leq \text{R}_{\rho}^{\text{sc}} \leq \text{Le}^{-1/2} \tag{2.7}$$

stable layering has to occur in the semi-convective regime (the upper limit is only approximate). The initial layering process is based on local breaking of gravity waves, often associated with the so-called Kato instability. Fig. 1 shows an advanced stage of layer formation in a simulation of semi-convection with the ANTARES code. A more detailed description of the simulation of such layers with this code is given below in Section 3.1.

SPRUIT (2013) derived a model for a more accurate prediction of the region where layer formation occurs that is expected to hold for arbitrary values of  $\text{Ra}_{\text{T}}$  and for  $\text{Pr} < 1$ . Numerical simulations by ZAUSSINGER and SPRUIT (2013) have shown that oscillatory instabilities are damped if  $\text{R}_{\rho}^{\text{sc}} \approx \text{Le}^{-1/2}$ , which results in very diffusive flows, while overturning cells are found to develop for values closer to 1. The prediction of SPRUIT (2013)

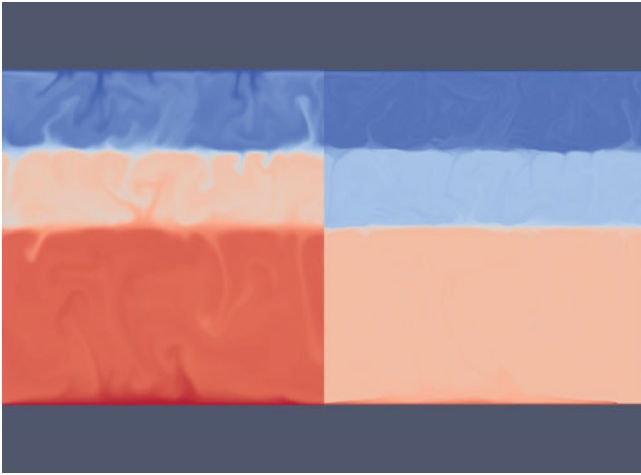


**Figure 1:** Layer formation in a snapshot of a simulation of semi-convection with idealized microphysics (constant diffusivities, Boussinesq approximation) in a 2D simulation with ANTARES. The parameters of the simulation are  $\text{Pr} = 1$ ,  $\text{Le} = 0.01$ ,  $R_\rho^{\text{sc}} = 3$ ,  $\text{Ra}_T = 5 \cdot 10^9$ . The left panel shows temperature, the right one salinity. The much sharper interfaces found for the latter are due to the very low diffusivity of the solute in comparison with heat, as follows from  $\text{Le} = 0.01 \ll 1$ . The blue color represents low values, red one high values with intermediate values encoded by bright, less intense colors.

of a critical maximum value of  $R_\rho^{\text{sc}}$  for layer formation, called  $R_{\rho\text{max}}^{\text{sc}}$ , was found to agree with the numerical simulations of ZAUSSINGER and SPRUIT (2013) within expected accuracy. For  $\text{Ra}_T = 10^6$ ,  $\text{Pr} = 1$ , and  $\text{Le} = 0.1$ , a value of  $R_{\rho\text{max}}^{\text{sc}} \approx 1.2$  is expected in comparison with  $R_{\rho\text{max}}^{\text{sc}} \approx 1.4$  which is actually found from numerical simulations. The model of SPRUIT (2013) also provides physical arguments to justify the following parametrization of thermal and solute fluxes by means of the Nusselt numbers for the semi-convective regime (i.e. turbulent fluxes in units of diffusive fluxes, for a detailed discussion see Section 4.1):

$$\text{Nu}_S - 1 = \frac{q}{\sqrt{\text{Le}} R_\rho} (\text{Nu}_T - 1). \quad (2.8)$$

Here,  $q$  is a fitting parameter in the quantitative comparison to numerical results and found to be close to 1. ZAUSSINGER and SPRUIT (2013) also find their numerical simulations of semiconvection to support such a parametrization. The layer thickness  $d$  itself depends mainly on the history of the system. Within the same modelling framework it can be estimated from the solute diffusivity for a time interval  $t$  as

$$d = \sqrt{2\kappa_S \text{Nu}_S t}. \quad (2.9)$$

It is limited from below by the length scale  $l_0$  on which the thermal diffusion time scale equals the free fall time over a pressure scale height (see ZAUSSINGER and SPRUIT, 2013),

$$l_0 = (\kappa_T^2 H_p / g)^{1/4} < d < H_p, \quad (2.10)$$

because on length scales smaller than  $l_0$  diffusion can exchange heat faster than convection. Moreover, the estimate has been derived under the Boussinesq approximation, which provides an upper limit for  $d$ . As is seen in laboratory experiments the layer thickness increases in time until a fully mixed single convection zone is established. However, to explain the continuous re-establishment of layers found in systems heated from the bottom, it may additionally be necessary to consider effects introduced by the assumed boundary conditions. Similar to the Rayleigh-Benard system the thermal Nusselt number can be estimated by a general power law,  $\text{Nu}_T = a(\text{Ra}_T \text{Pr})^b$ , but the exact values of  $a$  and  $b$  and their region of applicability are still a goal of ongoing research activities. Figs. 1 and 2 show the temporal evolution of a top and bottom bounded stratified fluid column with a fixed  $\Delta T$  and  $\Delta S$ . A steep initial temperature gradient at the bottom induced the development of plumes, forming the first layer. However, the solute is initially stratified linearly in the vertical direction. The height of the box is set to  $H = 5$ , for this multi-layer simulations, and to  $H = 1$  for single layer simulations. The Kato instability leads to three initial layers, which eventually merge into one single convective zone. The observed merging process happens on a single thermal (heat diffusion) time scale ( $t \leq \tau$ ).

### 2.2.3 Salt-fingering

We just briefly summarize the differences and similarities of the salt-fingering case in comparison with the semi-convective one. This process can occur despite the stratification is actually dynamically stable in the sense that a (vertically) displaced fluid parcel is restored back to its original position by buoyancy because  $\nabla_{\text{ad}} > \nabla$ , if there were no exchange of heat (and solute) with its (new) environment. For a real fluid with  $\text{Le} < 1$ , heat exchange by diffusion is faster than the corresponding exchange of solute. Then the heat exchange can lead to a net buoyancy force in the direction of the initial displacement. This is called *thermal* or *secular instability* (KIPPENHAHN and WEIGERT, 1991). In its initial phase this instability gives rise to a typical “fingering structure”. It may be triggered particularly easily, when the stable temperature gradient is counteracted by an unstable gradient in mean molecular weight ( $\nabla_\mu < 0$ ).

Again, the ratio of the gradients of mean molecular weight and potential temperature allows a distinction between a Ledoux stable and a Ledoux unstable case. In principle, one could use the definition of  $R_\rho^{\text{sc}} = \text{Ra}_S / \text{Ra}_T \approx \nabla_\mu / (\nabla - \nabla_{\text{ad}})$  to discuss salt-fingering (e.g., CANUTO, 1999), but here we use an alternative quantity more appropriate for the salt-finger case,  $R_\rho^{\text{sf}} = \text{Ra}_T / \text{Ra}_S \approx (\nabla - \nabla_{\text{ad}}) / \nabla_\mu$ , since it leads to symmetric relations.<sup>2</sup>

<sup>2</sup>The direct computation of the stability parameters  $R_\rho^{\text{sc}}$  and  $R_\rho^{\text{sf}}$  from temperature gradients is more convenient for the fully compressible case, for which the definition of the Rayleigh numbers can alternatively be defined in terms

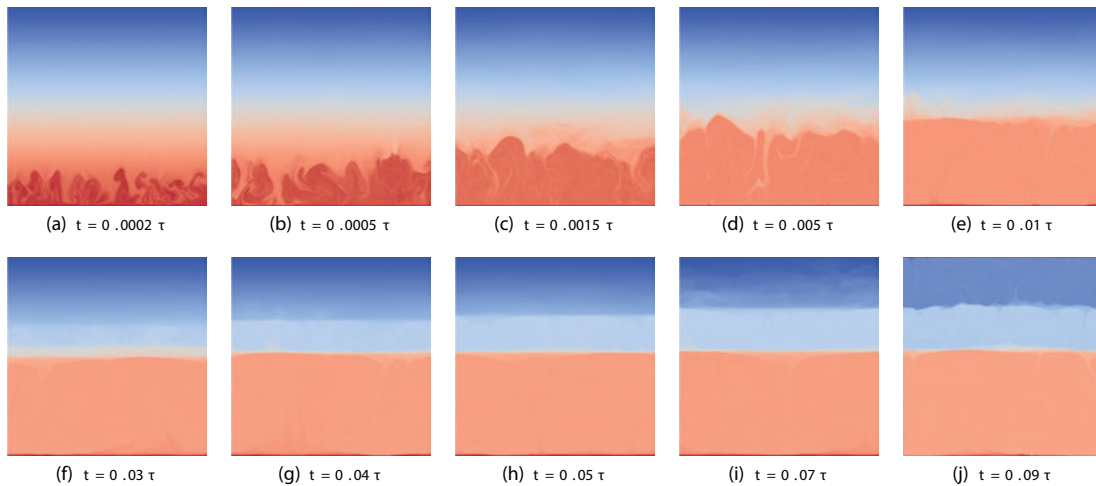


**Figure 2:** Temporal evolution of a semi-convective stack visualized for the solute. The steep temperature gradient at the bottom induces an initial layer, which grows until  $0.01\tau$  (upper row, panels a–e). However, the Kato oscillation triggers the evolution of the second and a third layer, (lower row, panels f–j). The lower row ranges from  $0.03\tau$  to  $0.09\tau$ , where  $\tau$  is the thermal diffusion time scale for the entire box. Each layer is convectively unstable. At least temporarily the thermal and solute transport from one layer to the next one is by diffusion only. The simulation parameters are  $Pr = 1$ ,  $Le = 0.01$ ,  $R_\rho^{sf} = 3$ ,  $Ra_T = 5 \cdot 10^9$ . The simulation has been computed using the ANTARES code.

In this case,  $R_\rho^{sf} < 1$  describes the Ledoux unstable case ( $N^2 < 0$  and  $\nabla - \nabla_{ad} > \nabla_\mu$ ) where the fluid is rapidly mixed and thus pre-existing gradients disappear unless they are maintained by the boundaries of the layer.  $R_\rho^{sf} > 1$  relates to the Ledoux stable case of salt-fingering which is of interest here, because the efficiency of mixing and the temporal development of the flow depend on the ratio of the different diffusivities (heat, concentration, momentum), and thus on  $Pr$  and  $Le$ . Linear stability analysis allows a first characterization of the Ledoux stable parameter regime and as for semi-convection the evolution time scale of a salt-fingering layer is the thermal diffusion time scale (at least if  $Le < 1$  and  $Pr < 1$ ). The actual stability criteria and mixing efficiencies depend on effective (turbulent) diffusivities (CANUTO, 1999) that can only be obtained from a (non-linear) model or a numerical simulation. As in semi-convective systems, the entire double-diffusive system evolves on time scales even longer than those of thermal diffusion, because the slower diffusion of the solute plays a role, too.

Fig. 3 shows two snapshots of a saltfinger simulation with the MITgcm code. The fingers appearing during early stages (100 sec, left panel) are much more distinct than the structures appearing during late stages. The domain was 24.75 cm in height and 8.25 cm in width. The simulation starts with a system of two clearly distinguishable layers. The temperature difference between lower and upper boundary was  $\Delta T = 1^\circ$  and chosen as described in Table 2 in Section 4. Late stages of the sim-

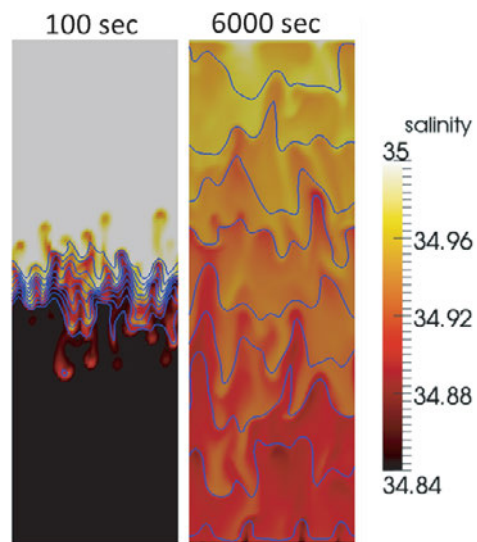


**Figure 3:** Snapshot of salinity distribution (colors) with temperature contours of  $\Delta T = 0.1^\circ$  within a saltfinger simulation with a stability ratio of  $R_\rho^{sf} = 1.33$  after 100 sec (left panel) when local instabilities start to develop and with well developed up- and downwelling (salt-) fingers after 6000 sec (right panel). The color scale for salinity is the same for both panels. The simulation has been performed with the MITgcm code.

of local gradients rather than through temperature or solute differences measured along a distance  $D$ . The definition of  $R_\rho^{sc}$  and  $R_\rho^{sf}$  through Rayleigh numbers is universal: it hides the difference about how the buoyancy frequency is computed in the Boussinesq case as opposed to the fully compressible one, where the Rayleigh number can be “local” or refer to average conditions in an entire layer.

ulation such as that one shown in the right-hand panel of Fig. 3 have already lost most information about their initial state and thus the latter would have looked quite similar in this sense if it had been started from a condition with constant initial gradients in  $T$  in  $S$  (cf. ZWEIFLE, 2011). A more detailed description of the evolution of such layers with this code is given in Section 3.2.

### 3 Numerical methods

In the following we describe the improvements made to the ANTARES simulation code, initially during the MetStröm project, and the setup of MITgcm, which were required for our studies of double-diffusive convection. Since this work is one of the essential results of the project and existing partial descriptions require to read selected parts of quite a few publications for a full account, we provide a complete summary and detailed references to each of the original papers in the following subsections.

#### 3.1 ANTARES

The ANTARES code (MUTHSAM et al., 2010) is a multi-purpose simulation program to solve the hydrodynamical conservation laws numerically in one, two, and three spatial dimensions. An initial state of the system can be evolved in time given various types of boundary conditions. The spatial discretization of advection operators (and in some cases also of pressure gradient operators) is based on the weighted essentially non-oscillatory scheme of 5th order (WENO5) proposed by JIANG and SHU (1996), optionally with Marquina flux splitting (DONAT and MARQUINA, 1996). Diffusion terms are discretized in a compatible way (HAPPENHOFER et al., 2013). Time integration is performed using strong stability preserving Runge–Kutta methods (SHU and OSHER, 1988, KRAAIJEVANGER, 1991, see also KUPKA et al., 2012). The code is fully parallelized following the MPI (message passing interface) paradigm (see MUTHSAM et al., 2010 for further details). With this framework implementation of an explicit time integration scheme for the Navier–Stokes equation augmented by an equation for the time evolution of concentration and the conservation laws for mass and energy, i.e. the system (2.1), was readily possible (ZAUSSINGER, 2010).

As mentioned in Section 2.1 the Boussinesq approximation is useful for basic explorations of double-diffusive convection. This holds in particular for comparisons with oceanographic cases. In ZAUSSINGER (2010) ANTARES was hence extended to solve the dynamical equations (2.2)–(2.3) or, in practice, (2.3)–(2.4). This setup differs from the compressible case by requiring the solution of a Poisson equation for the pressure fluctuations which ensures the incompressibility constraint (2.3) to hold during time integration. In ANTARES this is usually done with the FISHPACK solver of ADAMS et al. (2011), a fast finite difference based solver which has been parallelized by means of the Schur complement algorithm (GRIMM-STRELE, 2010) during the MetStröm project (ZAUSSINGER, 2010). A time split integration of (2.4) is performed where the velocity equation is first integrated in time without the pressure term, followed by the computation of pressure fluctuations under the constraint (2.3). Finally, the velocity field is corrected for the latter. Hence, the WENO5 discretization is only applied to the advection

terms in (2.4) given by their flux functions  $uS$ ,  $u \otimes u$ , and  $u\Theta$  and no transformation of the independent variables into their local characteristic fields is necessary to build up the WENO5 stencil. This is possible because the direction of the numerical flux along each Cartesian coordinate is uniquely determined by the sign of each velocity component. In conjunction with the excellent parallelization through the Schur complement approach an efficient and accurate method to solve (2.3)–(2.4) has been obtained and also successfully compared with direct solutions of (2.1) for a parameter region accessible to fully explicit time integration methods (ZAUSSINGER, 2010; ZAUSSINGER and SPRUIT, 2013).

For numerical simulations of double diffusive convection with ANTARES the vertical boundary conditions are usually taken to be impermeable for temperature and solute, respectively, as well as stress-free. This ignores the distortions of the interfaces by gravity waves. In the horizontal direction periodic conditions are chosen. The initial stratification depends on the investigated problem, however, linear or step-like initial stratifications are used in most cases. Simulations in the Boussinesq approximation require the specification of  $Le$ ,  $Pr$ ,  $Ra$ , and  $R_\rho$  (i.e. either  $R_\rho^{sc}$  or  $R_\rho^{sf}$ ). For the compressible case the depth of the domain in units of pressure scale heights has to be specified, too. The detailed algorithm for the setup of the initial stratification is described in ZAUSSINGER (2010) as well as in ZAUSSINGER and SPRUIT (2013). It is an extension of the procedure developed by MUTHSAM et al. (1995, 1999) for direct numerical simulations of compressible convection.

Simulations of double diffusive convection with a strong vertical stratification cannot rely on the Boussinesq approximation. In such cases the flow speed may become large, the mean stratification may no longer be constant with time, or (in a more general scenario) the diffusivities may be functions of temperature and chemical composition sufficiently sensitive to the variations induced by stratification and flow such that they can no longer be considered constant. One way to proceed in such cases is to consider analytical approximations to the fully compressible equations which are more refined than the Boussinesq approximation. KWATRA et al. (2009), however, developed an operator splitting method that integrates the pressure terms  $\nabla \cdot P$  and  $\nabla \cdot Pu$  in (2.1) in a semi-implicit manner without further approximations to the analytical equations themselves. The advection operators  $\nabla \cdot \rho u$ ,  $\nabla \cdot c\rho u$ ,  $\nabla \cdot \rho u \otimes u$ , and  $\nabla \cdot eu$  are integrated explicitly, while the time integration of the pressure terms requires the solution of a linear, generalized Helmholtz equation. This problem is only slightly more complex than the solution of a Poisson equation which appears during the numerical integration of (2.2)–(2.3). Full consistency with the equation of state is ensured here since the “predicted pressure” obtained from this elliptic equation is only used in an intermediate step. The physical pressure is recomputed at the end of each stage or step. In practice, no iterations on this step are required. As is the case for (2.2)–(2.3)



a transformation into local characteristic variables is not needed any more, because the sound speed no longer matters when determining the direction of the numerical flux at the boundary of a grid cell once the advection terms and the pressure terms are treated separately. [HAPPENHOFER et al. \(2013\)](#) demonstrated how to extend this method to the case of a two-species fluid under the presence of buoyancy and diffusion of heat and concentration, i.e. the full system (2.1). Strong scaling was demonstrated when a conjugate-gradient based solver for the solution of the generalized Helmholtz equation is combined with the Schur complement for parallelization ([HAPPENHOFER et al., 2013](#)). This was found to hold for three orders of magnitudes with respect to the number of processors, i.e. for up to more than 1000 CPU cores.

In numerical simulations of double diffusive convection the diffusive processes may set the most restrictive time step limit  $\Delta t$  for an explicit integration method. But as long as the flow velocities are small, the solution may actually change only by a little amount during  $\Delta t$ . Thus, implicit time integration methods may be desirable. At least in principle they allow increasing  $\Delta t$  such that the simulation proceeds with a time step corresponding to the change rate of the solution rather than that of an additive (and possibly negligibly small) contribution to it. Additive splitting techniques promise to be particularly efficient for the numerical integration of such problems: the non-linear advection operators offer very little potential for speed-up through implicit methods, because unless the problem is stationary, the solution is expected to vary significantly between two grid cells of size  $\Delta x$  over a time scale  $t = \Delta x/|u|$ . At the same time, the solution of a large, non-linear system of algebraic equations is expensive in terms of computing time. If instead only the terms related to diffusion are integrated by an implicit method, the ensuing (quasilinear and scalar) Helmholtz equations can be solved very efficiently. This has motivated the study and further improvement of implicit-explicit Runge-Kutta (IMEX RK) methods which are strong stability preserving (SSP). [KUPKA et al. \(2012\)](#) discussed the benefits of such integration methods for numerical simulations of double-diffusive convection. Combining them with semi-implicit methods for the time integration of pressure gradients for the compressible case ([HAPPENHOFER et al., 2013](#)) or the Boussinesq approximation removes the most severe time step limitations from numerical simulations of semi-convection and salt-fingers, at least for the case where  $Pr < 1$ . Through extension of this approach to a general additive splitting method, which is work in progress, the time integration can proceed along an optimum time step  $\Delta t$  without the undue costs of fully implicit time integration methods applied to (2.1) or (2.2)–(2.3).

ANTARES permits grid refinement as means of resolution optimization ([MUTHSAM et al., 2010](#)). Because the simulations of double-diffusive convection entail layer formation and merging as well as the formation, merging, and destruction of plumes, fine vortex structures, and other non-stationary features close to the limit of

grid resolution, predefined regions of high resolution are of limited use here. The simulations performed in this research have hence been done on single, fixed grids with a resolution optimized according to the physical diffusivities represented by the model equations.

We note that the results of all simulations discussed in the present paper which have been computed with ANTARES are based on the Boussinesq approximation and repeat that a comparison of these results with calculations based on the fully compressible Equations (2.1) was presented in [ZAUSSINGER \(2010\)](#) and [ZAUSSINGER and SPRUIT \(2013\)](#). The former also discusses an extensive grid of models assuming the Boussinesq approximation. That grid provides the basis for the extrapolations to the stellar case to which we turn in Section 4.3.

### 3.2 MITgcm

The Massachusetts Institute of Technology general circulation model (MITgcm) is a general purpose grid-point algorithm that solves the Boussinesq form of the Navier-Stokes equations for an incompressible fluid, here fully non-hydrostatic, with a spatial finite-volume discretization on a curvilinear computational grid (in the present context on a three-dimensional Cartesian grid). The model algorithm is described in [MARSHALL et al. \(1997\)](#); for online documentation and access to the model code, see [MITGCM GROUP \(2012\)](#). The code supports multi-threading and MPI for parallelization and also vector-cpu architectures; it has been shown to scale for order( $10^3$ ) CPUs ([HILL et al., 2007](#); [LOSCH et al., 2014](#)). Here, we use the MPI parallelization.

The MITgcm was originally built for large scale oceanographic and atmospheric applications, but the robust numerics and the non-hydrostatic extension of the solution algorithm (a pressure correction method) allows simulations of small scales with very high grid resolution (e.g. [LOSCH, 2004](#); [LOSCH et al., 2006](#); [ZWEIGLE, 2011](#)). The hydrostatic and non-hydrostatic pressure contributions are obtained from solving two- and three-dimensional elliptic problems implicitly with a preconditioned conjugate-gradient method. All other terms in (2.2) (or (2.5)) are stepped forward in time explicitly. For the direct numerical simulations (DNS) of semi-convection and salt fingering we make use of some of the specific features of the MITgcm, in particular, a 7th order monotonicity preserving advection scheme for tracers with very little numerical diffusion ([DARU and TENAUD, 2004](#)).

For the simulations of semi-convection with MITgcm which we show here, the model domain is a 384 mm by 128 mm water body (aspect ratio 3:1) with a grid spacing of 1 mm in all directions and periodic in the horizontal. The domain size is limited by computational requirements resources, but our domain already allows the formation of several convection cells. The simulations are practically 2D to save computer time, but we allow a

**Table 1:** Thermal and saline (solute) Rayleigh numbers of simulated semi-convection in the ocean and stability ratios. The Rayleigh numbers are calculated from values at the upper and lower boundaries. In all cases, the Lewis number was  $Le = 0.01$ .

	$R_\rho^{sc}$	$Ra_T$	$Ra_S$
SE-1	1.00	$2.96 \times 10^6$	$2.96 \times 10^6$
SE-2	1.02	$2.96 \times 10^6$	$3.02 \times 10^6$
SE-3	1.05	$2.96 \times 10^6$	$3.11 \times 10^6$
SE-4	1.10	$2.96 \times 10^6$	$3.26 \times 10^6$
SE-5	1.50	$2.96 \times 10^6$	$4.44 \times 10^6$
SE-6	2.00	$2.96 \times 10^6$	$5.92 \times 10^6$

few (10) grid points in the  $y$ -direction. FLANAGAN et al. (2013) show that, compared to true 3D-simulations, 2D-simulations of semi-convection tend to overestimate the effective fluxes for very low stability ratios  $R_\rho^{sc}$ . Still, they conclude that 2D DNS provide an “attractive alternative” to 3D DNS, at least for the region of applicability identified by comparisons with 3D simulations. The latter are important since the transport properties of 2D and 3D flow can be quite different, as also their results for low values of  $R_\rho^{sc}$  demonstrate. The size of the domain allows the formation of several convection cells. Temperature and salinity at the bottom and the uppermost layer are restored to the initial values in order to maintain the stratification and simulate an unlimited reservoir above and below. Explicit molecular diffusivities of  $\kappa_T = 1.5 \times 10^{-7} \text{ m}^2 \text{ s}^{-1}$  and  $\kappa_S = 1.5 \times 10^{-9} \text{ m}^2 \text{ s}^{-1}$ , and viscosity (diffusivity of momentum) of  $\nu = 9.3 \times 10^{-7} \text{ m}^2 \text{ s}^{-1}$  give realistic Prandtl and Lewis numbers of  $\sigma = \frac{\nu}{\kappa_T} = 6.2$  and  $Le = \frac{\kappa_S}{\kappa_T} = 0.01$ . The thermal diffusive time scale  $\tau$  is  $D^2/\kappa_T = (128 \text{ mm})^2/1.5 \times 10^{-7} \text{ m}^2 \text{ s}^{-1} \approx 30 \text{ h}$ . Several simulations with different boundary conditions are summarized in Table 1. All simulations start from step-like initial conditions, inspired by the layers that form in semi-convection (cf. Fig. 2(h) at  $t = 0.05\tau$ ). Without these initial conditions, the integrations would have to be very long and expensive. We note that we have focussed here on a parameter range with respect to  $R_\rho^{sc}$  which is dynamically the most interesting one. For smaller values of  $R_\rho^{sc}$  the results from linear stability analysis are rapidly recovered while the diffusive states typically found for larger values are computationally expensive and at the same time the predictions from stability analysis are the least certain ones for the intermediate values we have investigated here.

Fig. 4 shows a snapshot of a semi-convection simulation after 2700 sec und 6500 sec. Through the exchange of energy (heat), the boundary layer in the middle of the domain destabilizes and starts oscillating. These oscillations develop into approximately five convection cells that characterize the turbulent mixing process. The boundary layer between these convective (rolling) cells was preserved during the entire simulation.

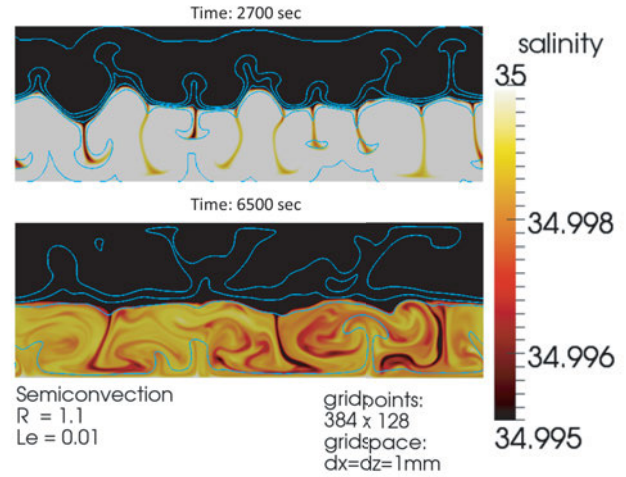


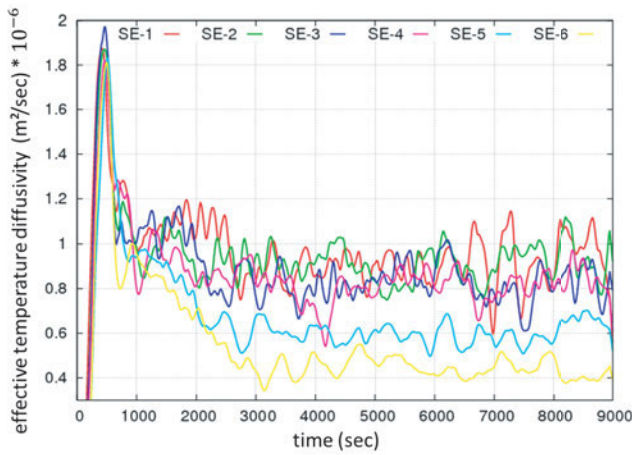
**Figure 4:** Snapshot of salinity distribution with temperature contours of  $\Delta T = 0.02^\circ$  within a simulation of semi-convection with stability ratio  $R_\rho^{sc} = 1.1$  after 2700 sec (upper panel) when local instabilities start to develop and with well developed (rolling) convection cells after 6500 sec (lower panel). The color scale of salinity is chosen to emphasize the structure of the lower fresh layer; similar patterns are found in the upper layer (not visible).

## 4 Results

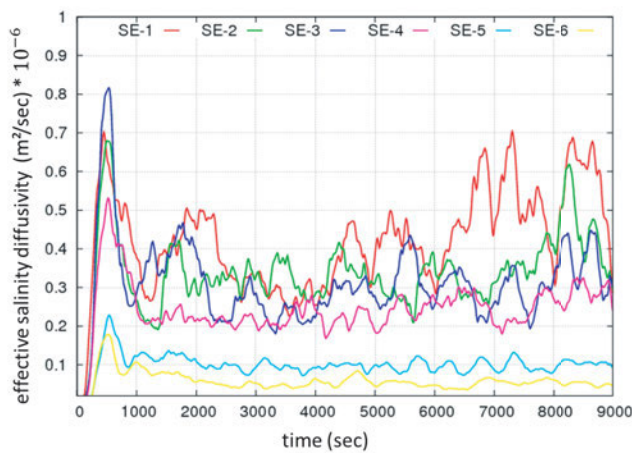
### 4.1 Effective diffusivities in the ocean

Vertically stratified fluids can release potential energy which eventually leads to (often turbulent) vertical fluxes of heat and concentration. Keeping the limitations of the diffusion approximation in mind the horizontal average of such fluxes,  $\overline{w'\chi'}$ , can also be described in terms of an effective diffusivity,  $K_\chi = \overline{w'\chi'}/(\partial_z \overline{\chi})$ , or through non-dimensionalized Nusselt numbers,  $Nu_\chi = (K_\chi)/(\kappa_\chi)$ . Here,  $\chi$  is supposed to mean either temperature  $T$ , adiabatically filtered temperature  $\Theta$ , or concentration (salinity)  $S$ .

If we consider the evolution of the numerical simulations summarized in Table 1 as a function of time, the effective diffusivities  $K_T$  and  $K_S$  turn out to reach a maximum near the end of the spin-up from the initial state. Then, especially for larger stability ratios, the system equilibrates at lower diffusivities (Fig. 5). To interpret these results we note that the effective diffusivities have been evaluated here as horizontal averages of fluxes across a horizontal section at the vertical middle of the domain, where the interface between the two layers of fluid is initially located. For this set of simulations the interface hardly changes its position with respect to its vertical location, as is also indicated by the stable (and stationary) horizontal averages of  $T$  and  $S$ , which explains the physical motivation behind this simple procedure. On the other hand, the background gradients  $\partial_z \overline{T}$  and  $\partial_z \overline{S}$  are computed from the vertical mean gradients of these quantities over the central 50% of the domain. We recall that  $T$  and  $S$  are kept fixed at the top and at the bottom of the simulation domain during these experiments.



(a)  $K_T^{SC}$  at interface with linear background gradients



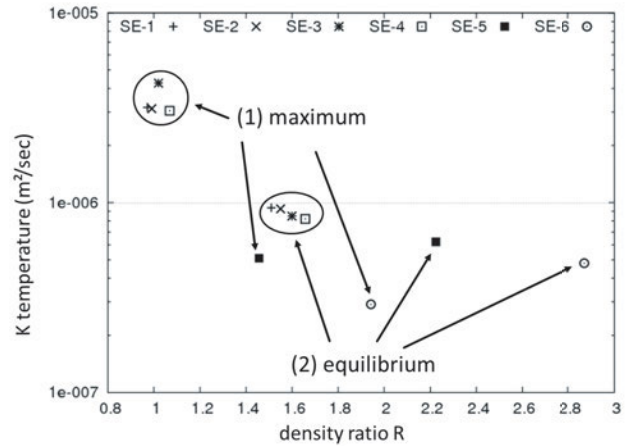
(b)  $K_S^{SC}$  at interface with linear background gradients

**Figure 5:** Temporal evolution of effective diffusivities smoothed with a running mean over 150 seconds. The different line colors refer to the experiments SE-1 to 6 in Table 1.

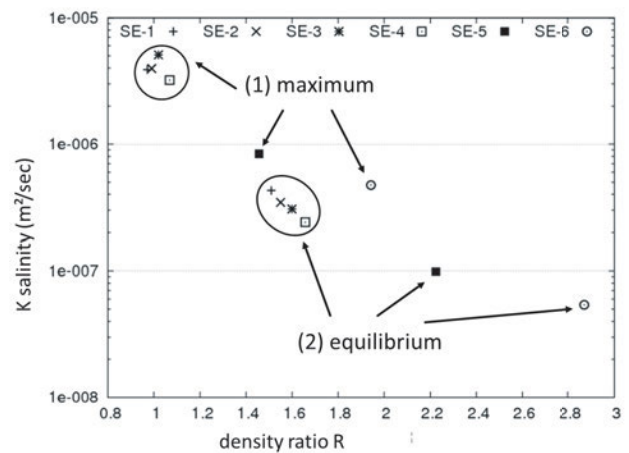
To show the temporal evolution of the effective diffusivities we have picked for Fig. 5 one horizontal level at the interface to compute the fluxes and their corresponding effective diffusivities to follow them (for the different simulations) as a function of time. We estimate the effective diffusivities twice per simulation: (1) when they reach their maximum values after about 500 seconds (Fig. 5) and (2) as the mean over the equilibrium phase when the convection cells have formed and  $R_{\rho,local}^{sc}$  along with the stability has increased.  $R_{\rho,local}^{sc}$  is evaluated from the background gradients computed over the central 50% of the domain rather than from taking the gradients over the entire domain, which are kept fixed due to the boundary conditions. It is hence a measure of local stability (cf. also Fig. 4.33a and Table 4.5 in ZWEIGLE (2011)).

In our simulations we obtain effective diffusivities within a range of  $K_T = 0.29$  to  $4.27 \cdot 10^{-6} \text{ m}^2/\text{s}$  and  $K_S = 0.054$  to  $5.09 \cdot 10^{-6} \text{ m}^2/\text{s}$ .

Based on the estimates of effective diffusivities, summarized in Fig. 6, we present a parametrization for the



(a)  $K_T^{SC}$  vs  $R_{\rho}^{sc}$



(b)  $K_S^{SC}$  vs  $R_{\rho}^{sc}$

**Figure 6:** Effective diffusivities estimated from simulations (1) when they are maximal, (2) as a mean over the equilibrium state. The different symbols refer to the experiments SE-1 to 6 in Table 1.

effective diffusivities of temperature and salinity,

$$K_T = \frac{\kappa_T}{a_1 + b_1 \ln(R_{\rho}^{sc})}, \quad (4.1)$$

$$K_S = K_T \mathcal{T}_{\text{turb}}, \quad (4.2)$$

with the turbulent Lewis number

$$\mathcal{T}_{\text{turb}} = \frac{c_2}{a_2 + b_2 R_{\rho}^{sc}}, \quad (4.3)$$

with  $a_1 \sim 0.06$ ,  $b_1 \sim 0.32$ ,  $a_2 \sim -3.7$ ,  $b_2 \sim 4.0$ , and  $c_2 \sim 0.1$ . This parametrization is only valid for stability ratios  $R_{\rho}^{sc} \in [1, 2.8]$ . In contrast with Eq. (2.7)–(2.10), the relations Eq. (4.1)–(4.3) are purely empirical fitting formulae. Note that some of the diffusivity estimates of type (1) (maximum values) overlap with those of type (2) (equilibrium phase) for less stable initial conditions suggesting that the parametrization may be more general.

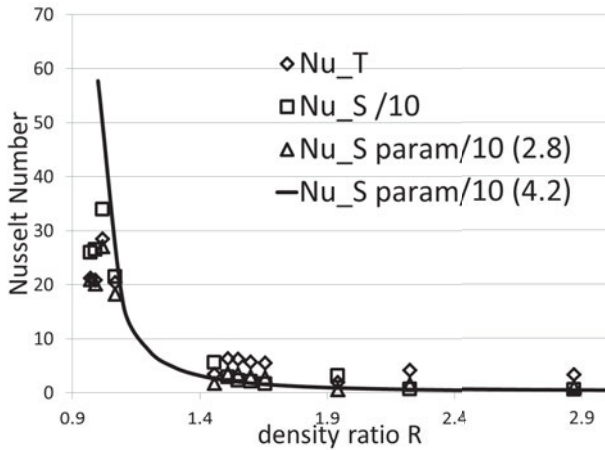


**Figure 7:** Thermal and saline (solute) Nusselt numbers  $Nu_T$  (diamonds) and  $Nu_S$  (squares) from simulation over density ratio  $R_\rho^{sc}$ . The saline Nusselt numbers are scaled down by a factor of 10. The Nusselt numbers derived from the simulations are compared to the saline Nusselt number computed from Equation (2.8) with  $q = O(1)$  (triangles) and computed from Equations (4.1) and (4.3) (line).

**Table 2:** Thermal and saline (solute) Rayleigh Numbers in a simulated saltfinger situation with  $Le = 0.1$ , stability ratios and Rayleigh numbers are comparable to the semi-convection case (see Table 1).

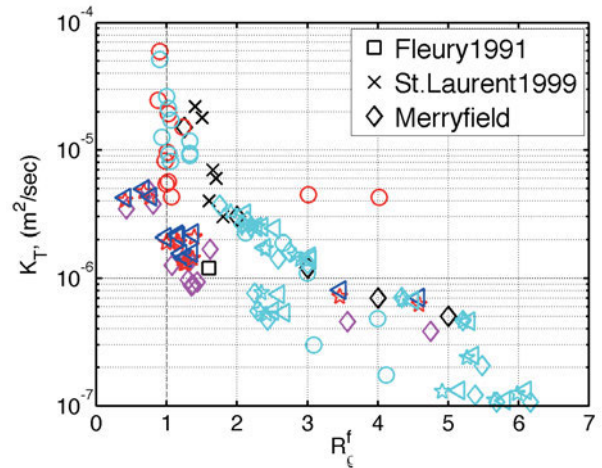
$R_\rho^{sf}$	$Ra_T$	$Ra_S$
1.33	$1.8 \times 10^8$	$1.35 \times 10^8$
1.33	$1.8 \times 10^8$	$1.35 \times 10^8$
1.06	$1.8 \times 10^8$	$1.65 \times 10^8$
2.16	$1.8 \times 10^8$	$0.8 \times 10^8$
2.66	$1.8 \times 10^8$	$0.65 \times 10^8$

Fig. 7 shows the simulated thermal and saline (solute) Nusselt numbers  $Nu_T$  and  $Nu_S$  obtained from the effective diffusivities by  $Nu_\chi = K_\chi/\kappa_\chi$ . The Nusselt numbers satisfy Equation (2.8) with  $q = O(1)$  (black triangles). The Nusselt numbers  $Nu_S$  computed with relationships (4.1) and (4.3) are drawn for reference (solid line in Fig. 7).

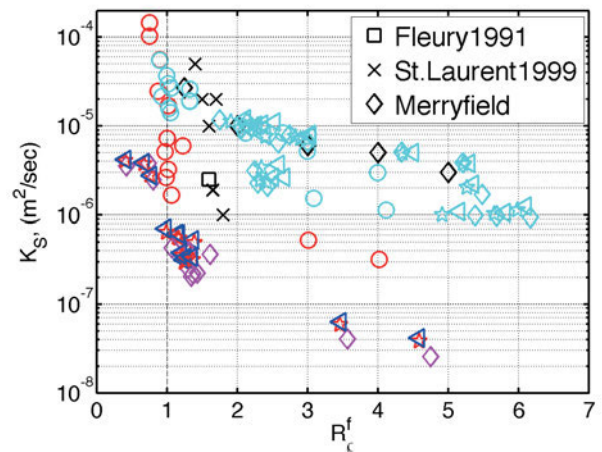
## 4.2 Comparison to salt fingering in the ocean

Several observational campaigns (MARMORINO et al., 1987; LAURENT and SCHMITT, 1999; POLZIN et al., 2001; BIANCHI et al., 2002), lab experiments (TAYLOR and BUCENS, 1989) and numerical simulation studies (ÖZGÖKMEK et al., 1998; YOSHIDA and NAGASHIMA, 2003; ZWEIGLE, 2011) shed light on the magnitude of fluxes in saltfingering. For semi-convection there are very few data available for comparison (TURNER, 2010; KELLY et al., 2003).

In the case of the ocean the effective diffusivity of temperature is of the same order of magnitude for both semi-convection and saltfingering (Fig. 8(a)) although the semi-convection diffusivities tend to be lower. However, we have found the effective diffusivity of salinity to



(a) Effective temperature diffusivities for semi-convection (red, blue, magenta) from our simulations and for saltfinger convection from our simulations (cyan) and by other authors (black) for comparison.



(b) Effective salinity diffusivities for semi-convection (red, blue, magenta) from our simulations and for saltfinger convection from our simulations (cyan) and by other authors (black) for comparison.

**Figure 8:** Collection of effective diffusivities from a variety of numerical experiments and field observations. (a) temperature diffusivities, (b) salinity diffusivities. Each of them is plotted as a function of the respective stability parameter  $R_\rho$ , i.e. either  $R_\rho^{sf}$  or  $R_\rho^{sc}$ . The cyan symbols represent values from numerical simulations of salt fingering (Table 2), the black symbols are estimates for salt fingering by other authors based on numerical simulations (MERRYFIELD, 2000 2002), or on observations (FLEURY and LUECK, 1991; LAURENT and SCHMITT, 1999). The effective diffusivities calculated from turbulent fluxes in semi-convection simulations (cf. Fig. 6) are represented by red, blue, and magenta symbols.

be smaller by one to two orders of magnitude for semi-convection in comparison with saltfingering in that case (Fig. 8(b)).

The explanation for the larger salt fluxes (and slightly bigger heat fluxes) in saltfingering follows from the nature of the instability as sketched in the introduction. In the saltfingering case, the differential diffusion represents a positive feedback and perturbations are acceler-

ated, as warm and saline water parcels from *above* loose heat and thus buoyancy and vice versa, cold and fresh waters from *below* gain heat and buoyancy. In contrast, perturbations in the semi-convection case are damped as warm and saline water parcels from *below* loose heat and thus buoyancy and vice versa, so that they are decelerated.

Hence, the differential diffusion in semi-convection leads to a negative feedback which in turn supports stable layers (such as those seen in Fig. 2). These layers form yet another impediment to mixing so that, while mixing may be efficient within layers, the transport is slowed down by diffusive transition zones in-between each convective layer.

The scenario of saltfingers is different from that of semi-convection because there are no diffusive interfaces through which salinity is transported very slowly. As a result salinity is transported much more efficiently in the saltfinger case. This is in agreement with another finding of ZWEIGLE (2011): for saltfingers the turbulent fluxes found in the numerical simulations with the MIT-gcm depend only weakly on the Lewis number as long as the mixing processes have not changed the stratification to such an extent that the diffusion begins to dominate transports.

### 4.3 Extrapolation to stars

To estimate the range of parameter values for semiconvection zones in main sequence stars,<sup>3</sup> we have to quantify their physical state and compute the according diffusivities. If we use standard stellar evolution models, we obtain microscopic diffusivities of  $\kappa_T = 3 \cdot 10^4 \text{ m}^2 \text{ s}^{-1}$  and  $\kappa_{\text{He}} = 10^{-4} \text{ m}^2 \text{ s}^{-1}$  for the region of interest which itself has a typical height of  $H \sim H_p = 2 \cdot 10^8 \text{ m}$ . The values of these quantities are based on a  $15 M_\odot$  stellar evolution simulation kindly provided by A. WEISS. We can use Equations (2.7)–(2.10) to estimate the properties of the semi-convection zone. The Rayleigh number can be found as a function of the layer thickness  $d$  and the pressure scale height  $H_p$ . We obtain a modified Rayleigh number  $Ra^* = Ra \cdot Pr = 10^{12}$  for  $d/H_p = 0.1$  and  $Ra^* = 10^8/Pr$  for  $d/H_p = 0.01$ . The effective Helium diffusivity is found to be  $K_{\text{He}} = 10^{-1} \text{ m}^2 \text{ s}^{-1}$ , three orders of magnitudes above the microscopic diffusivity. This result is not surprising since the saline (solute) Nusselt number is found to be in the order of  $Nu_S = 10^3\text{--}10^4$ . These estimates are supported by numerical simulations (cf. Fig. 9) for a perfect gas equation of state and Prandtl numbers between 0.01 and 1.0 (see also (ZAUSSINGER, 2010; ZAUSSINGER and SPRUIT, 2013)). The estimates lead to a total mixing time scale of about  $10^{10} \text{ yr}$ . This is much longer than the time that stars with sufficient mass to feature semiconvection in their interior actually remain on the main sequence during their evolution

<sup>3</sup>stars for which nuclear fusion of hydrogen in their central region provides the main source of energy

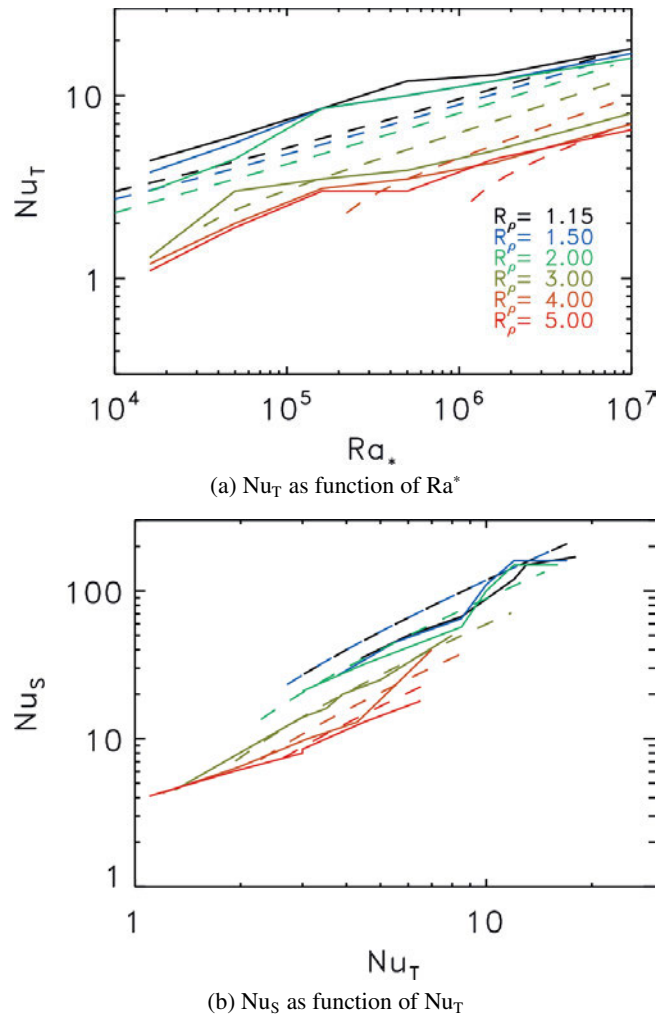


**Figure 9:** Dependence of the thermal Nusselt number on the modified Rayleigh number  $Ra^* = Ra \cdot Pr$  and the saline (solute) Nusselt number  $Nu_S$  for varying stability parameters  $R_p := R_p^c$ . The solid lines are numerical results for  $Le = 10^{-2}$ , dashed lines are model predictions.

(cf. (SALARIS and CASSISI, 2005)). The value of the initial layer thickness  $l_0 = 2 \cdot 10^3 \text{ m}$  is established in about some days, however, which is very short compared to an overall evolution time of more than  $10^7$  years (see also (ZAUSSINGER, 2010; ZAUSSINGER and SPRUIT, 2013)). The enormous differences in the timescales are mainly due to the extremely small value of the stellar Lewis number,  $Le \leq 10^{-9}$ . The same estimation can be done for layering processes in volcanic lakes (e.g. Lake Kivu) resulting in merging time scales of some months and an initial layer thickness of  $l_0 = 5 \text{ mm}$ .

Is the extrapolation over so many orders of magnitudes from direct numerical simulations to the stellar case reliable? The stellar case differs from the geophysical one by a very low kinematic viscosity compared to its much larger radiative diffusivity. This explains the very low values of  $Pr$ : the radiative diffusion inside a star in most ranges of temperature and density predom-

inates over contributions from particle collisions. Thermal boundary layers are thus much larger than the viscous ones and solute boundary layers are even smaller. Simulations used for extrapolation to the stellar regime should thus feature  $Le \ll Pr \ll 1$ . In practice, a best effort of  $Le \leq 0.1 \cdot Pr \leq 0.1$  can be achieved though quite often further compromises have to be made. At the least, the correct ordering of physical processes taking place on larger or smaller length scales when compared to each other can be ensured. We thus expect the idealized simulations to relate to the physical parameter of interest in the same sense as well-resolved large eddy simulations should do. Accepting this level of uncertainty we may thus extrapolate our results to the stellar parameter regime. Moreover, the extrapolation can be based on a physical model (SPRUIT, 2013) underlying (2.8) as long as this model compares sufficiently well with the simulations in the parameter regime that can be investigated directly. Currently, there is no known physical reason why the model (2.8) should break down just because of lowering  $Pr$  and  $Le$ .

The modified Rayleigh number  $Ra^* = Pr \cdot Ra_T$  plays a central role in comparing both regimes. In this context, the Prandtl- and the thermal Rayleigh number in both regimes require attention. The Prandtl number in semi-convective zones of stars is of the order of  $10^{-7}$ . The Rayleigh number, which scales with the third power of the height, is limited by  $10^4 < Ra_T < 10^{20}$ , resulting in  $10^{-3} < Ra^* < 10^{13}$ . A comparable value for double-diffusive layers in saltwater is about  $Ra^* = 10^9$ . This leads to a broad overlapping range of  $Ra^*$  and consequently the possibility to compare both regimes. The Prandtl number remains as the only uncertain parameter, but we could not observe a strong dependency in the depicted parameter range of  $Ra^*$  and  $Pr$  on the Nusselt numbers and hence on the convective fluxes. This result coincides with the theoretical estimation in SPRUIT (2013) and ZAUSSINGER and SPRUIT (2013).

Fig. 9 shows numerical and theoretical results of the relation between the thermal and solute fluxes parametrised in terms of the Nusselt numbers. The power law for double-diffusive (semi-) convection as derived and tested in ZAUSSINGER (2010) and ZAUSSINGER and SPRUIT (2013) fits over a broad range with numerical simulations, as is demonstrated in Fig. 9(a). However, the stability parameter  $R_\rho^{sc}$  plays a central role, which is not covered by the linear stability analysis. Fig. 9(b) depicts the dependency of the Nusselt numbers, which are related by the square root of the Lewis number (see Equation (2.8)). Even this relation is influenced by the stability parameter.

At the bottom line the mixing due to semi-convection is concluded to be a highly inefficient process over stellar evolution time scales (see ZAUSSINGER, 2010; ZAUSSINGER and SPRUIT, 2013) and if a higher mixing rate were required from astrophysical constraints in layers where semi-convection occurs, additional sources of mixing would have to be found.

## 5 Conclusions

In spite of the largely different geometrical scales, double-diffusive mixing processes in stars and in the ocean have several aspects in common. In both systems the molecular diffusion of concentration occurs much more slowly than the diffusion of heat. As a consequence, the formation of specific geometrical structures such as “salt-fingers” or “thermohaline staircases” is not restricted to the oceanographic scenarios and some laboratory counterparts for which these phenomena have originally been observed, but can also occur in other physical systems for which comparable ratios of diffusivities, temperature to concentration gradients, and buoyancy to diffusive time scales hold. In particular, convection inside stars and especially gaseous giant planets may have similar properties.

A numerical simulation of double-diffusive mixing processes either in oceans or in stars involves an enormous range of spatial and temporal scales. Hence, such a simulation will inevitably have some restrictions to its physical realism. State-of-the-art numerical algorithms can help to reduce such limitations. During the Met-Ström project the ANTARES and MITgcm simulation codes have been extended to make them applicable to direct numerical simulation of double-diffusive convection (ZAUSSINGER, 2010; ZWEIGLE, 2011). For the case of ANTARES numerical methods have been extended (HAPPENHOFER et al., 2013) and even the development of new time integration methods has been motivated (KUPKA et al., 2012; HIGUERAS et al., 2014). For astrophysical problems the focus during the project has been on semiconvection (or diffusive convection) where a stabilizing gradient in mean molecular weight counteracts a destabilizing temperature gradient (see ZAUSSINGER, 2010; ZAUSSINGER and SPRUIT, 2013). For oceanographic research the focus in the project has been on the case of salt-fingers (see ZWEIGLE, 2011).

In this paper we discussed some results of both projects on semiconvection in parameter spaces of interest to both astrophysics and oceanography. In either system the mixing efficiency is limited by sharp layer interfaces in the background stratification which tend to damp instabilities. These layers themselves develop from smooth background stratifications that favor semi-convection. The layers show a long life time (cf. ZAUSSINGER and SPRUIT, 2013 for estimates) although ultimately, after initial formation, merging processes occur (cf. also Fig. 2). The complementary double diffusive process of salt fingering leads to effective diffusivities for salinity that are one to two orders of magnitude higher than for semi-convection (see Fig. 8).

For both stellar and oceanic regimes, the scaled effective diffusivities (the Nusselt numbers) are found to follow approximately relationship (2.8). However, for the oceanographic case a purely empirical parametrization, (4.1)–(4.3), is also able to approximate fairly well the data on semiconvection from both measurements and our numerical simulations to within measurement uncer-

tainties in spite of its different dependence on the Lewis number  $Le$  (Fig. 7 and 8). Given the limited parameter range of the available simulations as a function of  $Le$  and the density ratio  $R_\rho^{sc}$ , more extended studies appear necessary that will clarify in greater detail the relationship of the effective diffusivities  $K_T$  and  $K_S$  to the basic physical parameters  $Le$ ,  $R_\rho^{sc}$  (as well as  $Pr$ ,  $Ra_T$ ) and also quantify more accurately the influence of boundary conditions or dimensionality (two vs. three spatial dimensions) on the results as is claimed in recent work of FLANAGAN et al. (2013). ANTARES and MITgem could readily be used for such studies to further explore the range of applicability of models such as (2.8).

## Acknowledgements

This research has been supported by the DFG within the projects “Modelling of diffusive and double-diffusive convection”, projects KU 1954/3-1 and LO 1143/3-1 in SPP 1276/1 and KU 1954/3-2 and LO 1143/3-2 in SPP 1276/2 within the interdisciplinary MetStröm project. F. ZAUSSINGER has also been supported by the Austrian Science Fund FWF through project P20973 (project leader H.J. MUTHSAM). F. KUPKA is grateful for support by the FWF through projects P21742 and P25229 (project leader). We thank A. WEISS, MPI for Astrophysics, Garching, for providing a stellar evolution model used in this research.

## References

- ADAMS, J., P. SWARZTRAUBER, R. SWEET, 2011: Efficient Fortran subprograms for the solution of separable elliptic partial differential equations. – Available at <http://www2.cisl.ucar.edu/resources/legacy/fishpack>.
- BAINES, P., A. GILL, 1969: On thermohaline convection with linear gradients. – *J. Fluid Mech.* **37**, 289–306.
- BIANCHI, A.A., A.R. PIOLA, G.J. COLLINO, 2002: Evidence of double diffusion in the Brazil–Malvinas confluence. – *Deep Sea Res.* **49**, 41–52.
- CANUTO, V., 1999: Turbulence in stars. III. Unified treatment of diffusion, convection, semiconvection, salt fingers, and differential rotation. – *Astrophys. J.* **524**, 311–340.
- CANUTO, V., 2011: Stellar mixing II. Double diffusion processes. – *Astron. & Astrophys.* **528**, A77.
- CARNIEL, S., M. SCLAVO, L. KANTHA, H. PRANDKE, 2008: Double-diffusive layers in the Adriatic Sea. – *Geophys. Res. Lett.* **35**, L02605.
- DARU, H., C. TENAUD, 2004: High order one-step monotonicity-preserving schemes for unsteady compressible flow calculations. – *J. Comp. Phys.* **193**, 563–594.
- DONAT, R., A. MARQUINA, 1996: Capturing shock reflections: An improved flux formula. – *J. Comp. Phys.* **125**, 42–58.
- FLANAGAN, J.D., A.S. LEFLER, T. RADKO, 2013: Heat transport through diffusive interfaces. – *Geophys. Res. Lett.* **40**, 2466–2470.
- FLEURY, M., R. LUECK, 1991: Fluxes across a thermohaline interface. – *Deep Sea Res.* **38**, 745–769.
- GRIMM-STRELE, H., 2010: Numerical solution of the Generalised Poisson Equation on Parallel Computers Master’s thesis, University of Vienna. – Available from <http://othes.univie.ac.at/9200/>.
- HAPPENHOFER, N., H. GRIMM-STRELE, F. KUPKA, B. LÖW-BASELLI, H. MUTHSAM, 2013: A low Mach number solver: Enhancing applicability. – *J. Comp. Phys.* **236**, 96–118.
- HIGUERAS, I., N. HAPPENHOFER, O. KOCH, F. KUPKA, 2014: Optimized strong stability preserving IMEX Runge–Kutta methods. – *J. Comp. Appl. Math.* **272**, 116–140.
- HILL, C., D. MENEMENLIS, B. CIOTTI, C. HENZE, 2007: Investigating solution convergence in a global ocean model using a 2048-processor cluster of distributed shared memory machines. – *Scientific Programming Programming* **12**, 107–115.
- HUPPERT, H.E., D. MOORE, 1976: Nonlinear double-diffusive convection. – *J. Fluid Mech.* **78**, 821–854.
- JIANG, G.-S., C.-W. SHU, 1996: Efficient implementation of weighted ENO schemes. – *J. Comp. Phys.* **126**, 202–228.
- KELLY, P.D.E., H.J.S. FERNANDO, A.E. GARGETT, J. TANNY, E. ÖZSOY, 2003: The diffusive regime of double-diffusive convection. – *Prog. Oceanogr.* **56**, 461–481.
- KIPPENHAHN, R., A. WEIGERT, 1991: *Stellar Structure and Evolution*. – Springer Verlag, Berlin.
- KRAAIJEVANGER, J., 1991: Contractivity of Runge–Kutta methods. – *BIT* **31**, 482–528.
- KUPKA, F., N. HAPPENHOFER, I. HIGUERAS, O. KOCH, 2012: Total-variation-diminishing implicit-explicit Runge–Kutta methods for the simulation of double-diffusive convection in astrophysics. – *J. Comp. Phys.* **231**, 3561–3586.
- KWATRA, N., J. SU, J. GRÉTARSSON, R. FEDKIW, 2009: A method for avoiding the acoustic time step restriction in compressible flow. – *J. Comp. Phys.* **228**, 4146–4161.
- LAURENT, L.S., R. SCHMITT, 1999: The contribution of salt fingers to vertical mixing in the North Atlantic Tracer Release Experiment. – *J. Phys. Oceanogr.* **29**, 1404–1424.
- LECONTE, J., G. CHABRIER, 2012: A new vision of giant planet interiors: Impact of double diffusive convection. – *Astron. & Astrophys.* **540**, A20.
- LECONTE, J., G. CHABRIER, 2013: Layered convection as the origin of Saturn’s luminosity anomaly. – *Nature Geosci.* **6**, 347–350.
- LEDOUX, P., 1947: Stellar models with convection and with discontinuity of the mean molecular weight. – *Astrophys. J.* **105**, 305–321.
- LESEUR, M., 1997: *Turbulence in Fluids*. – Kluwer Academic Publishers, Dordrecht.
- LINDEN, P.F., 1974: A note on the transport across a diffusive interface. – *Deep Sea Res.* **21**, 283–287.
- LOSCH, M., 2004: On the validity of the Millionschikov quasinormality hypothesis for open-ocean deep convection. – *Geophys. Res. Lett.* **31**, L23301.
- LOSCH, M., S. HERLUFSEN, R. TIMMERMANN, 2006: Effects of heterogeneous surface boundary conditions on parameterized oceanic deep convection. – *Ocean Model.* **13**, 156–165.
- LOSCH, M., A. FUCHS, J.-F. LEMIEUX, A. VANSELOW, 2014: A parallel Jacobian-free Newton–Krylov solver for a coupled sea ice–ocean model. – *J. Comp. Phys.* **257**(A), 901–910.
- MARMORINO, G., W. BROWN, W. MORRIS, 1987: Two-dimensional temperature structure in the C-SALT thermohaline staircase. – *Deep Sea Res.* **34**, 1667–1676.
- MARSHALL, J., A. ADCROFT, C. HILL, L. PERELMAN, C. HEISEY, 1997: A finite-volume, incompressible Navier Stokes model for studies of the ocean on parallel computers. – *J. Geophys. Res.* **102**(C3), 5753–5766.
- MCDUGALL, T.J., D.R. JACKETT, D.G. WRIGHT, R. FEISTEL, 2003: Accurate and computationally efficient algorithms for potential temperature and density of seawater. – *J. Atmos. Oceanic Techn.* **20**, 730–741.
- MERRYFIELD, W.J., 2000: Origin of thermohaline staircases. – *J. Phys. Oceanogr.* **30**, 1046–1068.

- MERRYFIELD, W.J., 2002: Intrusions in double-diffusively stable arctic waters: Evidence for differential mixing. – *J. Phys. Oceanogr.* **32**, 1452–1459.
- MIROUH, G.M., P. GARAUD, S. STELLMACH, A.L. TRAXLER, T.S. WOOD, 2012: A new model for mixing by double-diffusive convection (semi-convection): The conditions for layer formation. – *Astrophys. J.* **750**, 61.
- MITGCM GROUP, 2012: MITgcm User Manual. – Online documentation, MIT/EAPS, Cambridge, MA 02139, USA, [http://mitgcm.org/public/r2\\_manual/latest/online\\_documents](http://mitgcm.org/public/r2_manual/latest/online_documents).
- MUTHSAM, H., W. GÖB, F. KUPKA, W. LIEBICH, J. ZÖCHLING, 1995: A numerical study of compressible convection. – *Astron. & Astrophys.* **293**, 127–141.
- MUTHSAM, H., W. GÖB, F. KUPKA, W. LIEBICH, 1999: Interacting convection zones. – *New Astron.* **4**, 405–417.
- MUTHSAM, H., F. KUPKA, B. LÖW-BASELLI, C. OBERTSCHEIDER, M. LANGER, P. LENZ, 2010: ANTARES – A Numerical Tool for Astrophysical REsearch with applications to solar granulation. – *New Astron.* **15**, 460–475.
- ONKEN, R., E. BRAMBILLA, 2003: Double diffusion in the Mediterranean Sea: Observation and parameterization of salt finger convection. – *J. Geophys. Res.* **108**(C9), 8124.
- ÖZGÖKMEN, T.M., O.E. ESENKOV, D.B. OLSON, 1998: A numerical study of layer formation due to fingers in double-diffusive convection in a vertically-bounded domain. – *J. Marine Res.* **56**, 463–487.
- POLZIN, K., R. SCHMITT, J. TOOLE, 2001: SFTRE1 and SFTRE2, Woods Hole Oceanographic Institution. – <http://hrp.whoi.edu/hrpgrp/hrp.html>.
- PROCTOR, M., 1981: Steady subcritical thermohaline convection. – *J. Fluid Mech.* **105**, 507–521.
- RADKO, T., 2003: A mechanism for layer formation in a double-diffusive fluid. – *J. Fluid Mech.* **497**, 356–380.
- SALARIS, M., S. CASSISI, 2005: *Evolution of Stars and Stellar Populations* – Wiley, Chichester, England.
- SCHMID, M., M. BUSBRIDGE, A. WÜEST, 2010: Double-diffusive convection in Lake Kivu. – *Limnol. Oceanogr.* **55**, 225–238.
- SCHMITT, R.W., 1988: Mixing in a thermohaline staircase, in small-scale turbulence and mixing in the ocean. – Elsevier, New York, 435–452.
- SCHMITT, R.W., 2005: Enhanced diapycnal mixing by salt fingers in the thermocline of the tropical Atlantic. – *Science* **308**, 685–688.
- SCHWARZSCHILD, K., 1906: On the equilibrium of the Sun's atmosphere. – *Nachr. K. Ges. Wiss. Gött.* **195**, 41–53.
- SCHWARZSCHILD, M., R. HÄRM, 1958: Evolution of very massive stars. – *Astrophys. J.* **128**, 348–360.
- SHU, C.-W., S. OSHER, 1988: Efficient implementation of essentially non-oscillatory shock-capturing schemes. – *J. Comp. Phys.* **77**, 439–471.
- SPIEGEL, E.A., G. VERONIS, 1960: On the Boussinesq approximation for a compressible fluid. – *Astrophys. J.* **131**, 442–447.
- SPRUIT, H., 2013: Semiconvection: theory. – *Astron. & Astrophys.* **552**, A76.
- STERN, M.E., 1960: The “salt-fountain” and thermohaline convection. – *Tellus* **12**, 172–175.
- STEVENSON, D.J., 1979: Semiconvection as the occasional breaking of weakly amplified internal waves. – *Mon. Not. Roy. Astron. Soc.* **187**, 129–144.
- STEVENSON, D.J., 1985: Cosmochemistry and structure of the giant planets and their satellites. – *Tellus* **62**, 4–15.
- STOTHERS, R., N.R. SIMON, 1969: An explanation for the blue sequence of variable stars. – *Astrophys. J.* **157**, 673–681.
- TAYLOR, J.R., P. BUCENS, 1989: Laboratory experiments on the structure of salt fingers. – *Deep Sea Res.* **16**, 1675–1704.
- THOMAS, H.-C., 1967: Sternentwicklung VIII. Der Helium-Flash bei einem Stern von 1.3 Sonnenmassen. – *Z. Astrophys.* **67**, 420–455.
- TRAXLER, A., S. STELLMACH, P. GARAUD, T. RADKO, N. BRUMMELL, 2011: Dynamics of fingering convection. Part 1 small-scale fluxes and large-scale instabilities. – *J. Fluid Mech.* **677**, 530–553.
- TURNER, J.S., 1965: The coupled turbulent transports of salt and heat across a sharp density interface. – *Int. J. Heat Mass Transfer* **8**, 759–767.
- TURNER, J.S., 2010: The melting of ice in the arctic ocean: The influence of double-diffusive transport of heat from below. – *J. Phys. Oceanogr.* **40**, 249–256.
- VERONIS, G., 1965: On finite amplitude instability in thermohaline convection. – *J. Marine Res.* **23**, 1–17.
- YOSHIDA, J., H. NAGASHIMA, 2003: Numerical experiments on salt-finger convection. – *Progress Oceanogr.* **56**, 435–495.
- ZAUSSINGER, F., 2010: Numerical simulation of double-diffusive convection Ph.D. thesis, University of Vienna. – Available at <http://othes.univie.ac.at/13172/>.
- ZAUSSINGER, F., H. SPRUIT, 2013: Semiconvection: numerical simulations. – *Astron. & Astrophys.* **554**, A119.
- ZAUSSINGER, F., F. KUPKA, H. MUTHSAM, 2013: Semiconvection. – In: GOUPIL, M., K. BELKACEM, C. NEINER, F. LIGNIÈRES, and J. GREEN (Eds.), *Studying Stellar Rotation and Convection: Theoretical Background and Seismic Diagnostic*. – *Lecture Notes in Physics* **865**, Springer Verlag, Berlin, 219–237.
- ZODIATIS, G., G.P. GASPARINI, 1996: Thermohaline staircase formations in the Tyrrhenian Sea. – *Deep Sea Res.* **43**, 655–678.
- ZWEIGLE, T., 2011: Numerische Simulation von Salz fingern. – Ph.D. thesis, University Bremen, Department of Physics and Electrical Engineering, Germany. – Available at <http://epic.awi.de/33251/1/00102187-1.pdf>.